Electron spin dynamics and spin-lattice relaxation of trityl radicals in frozen solutions

Hanjiao Chen,[a] Alexander G. Maryasov,[b] Olga Yu. Rogozhnikova,[c,d] Dmitry V. Trukhin,[c,d] Victor M. Tormyshev[c,d] and Michael K. Bowman*[a]

[a] Department of Chemistry, The University of Alabama, Box 870336, Tuscaloosa, Alabama 35487-0336 USA.
[b] V. V. Voevodsky Institute of Chemical Kinetics and Combustion, 3 Institutskaya, 630090 Novosibirsk, Russia.
[c] N. N. Vorozhtsov Novosibirsk Institute of Organic Chemistry, 9 Academician Lavrentiev Ave., Novosibirsk 630090, Russia
[d] Novosibirsk State University, 2 Pirogova St., Novosibirsk 630090, Russia.

S 1 Saturation Bandwidth

The bandwidth saturated by the picket fence used in the saturation recovery measurements was determined in an ELDOR measurement. The microwave frequency of the picket fence was shifted from the detection frequency by using the ELDOR channel to produce the picket fence. The normalized saturation of the EPR signal was determined from the signal remaining immediately following the picket fence as the saturating frequency was shifted as far as 130 MHz from measurement frequency and the center of the spectrum.
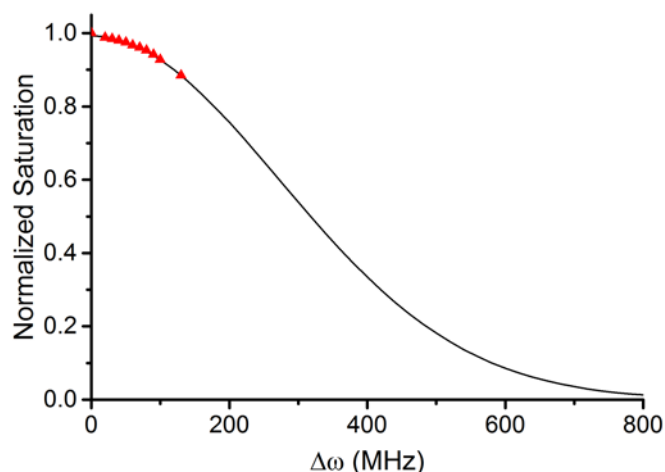

Figure S 1 Saturation bandwidth of 40 mM OX063 at 40 K and X-band. The red triangles are the measured saturation of the OX063 as the microwave frequency of the saturating picket fence was moved from the center of the EPR line. The solid black line is a least-squares fit of a Gaussian to the data with a full width at half maximum of 638 MHz.

The normalized saturation was fit well by a Gaussian curve with a full width at half maximum of 638 MHz. More than 90% saturation was achieved over a ±120 MHz range which is more than enough to saturate the entire EPR spectrum of Finland trityl or OX063. The largest ^{13}C hyperfine tensor element of 160.1 MHz was measured by CW-EPR for the parallel component of the hyperfine coupling of the central carbon in Finland trityl[1] and we have observed similar values in OX063. The next largest coupling is under 40 MHz, so the largest spectral extent in a trityl with two ^{13}C in natural abundance is less than 200 MHz or ±100 MHz relative to the center. There is also some broadening of the EPR spectrum from g-factor anisotropy which would contribute about 0.5 MHz broadening for every GHz of EPR frequency.[2, 3]

Similar saturation bandwidths could be achieved at W-band because of the greater bandwidth of the resonator. The picket fence used in our relaxation measurements provides a fairly uniform saturation of the entire observable EPR spectrum, although its performance at very large offsets is expected to deviate from the Gaussian fit.

S 2 Rate comparison with Filibian et al.

The T_{1e} of 15 mM OX063 in pyruvic acid was reported by Filibian et al.[4] at W-band for temperatures between 1.8-4.2K. They reported $1/T_{1e} = 0.23 \cdot T^{2.17}$ over this temperature range, which is difficult to compare directly with our results in terms of eq. (2).

However, plotting the curve for 15 mM OX063 in pyruvic acid with the curves fit to 50 mM Finland trityl in 60:40 glycerol:H_2O, Figure S 2, shows excellent agreement in both the temperature dependence of $1/T_{1e}$ and the overall magnitude. It appears that the function obtained by Filibian et al. is just the tangent to the relaxation rate in the 1.8-4.2 K region.
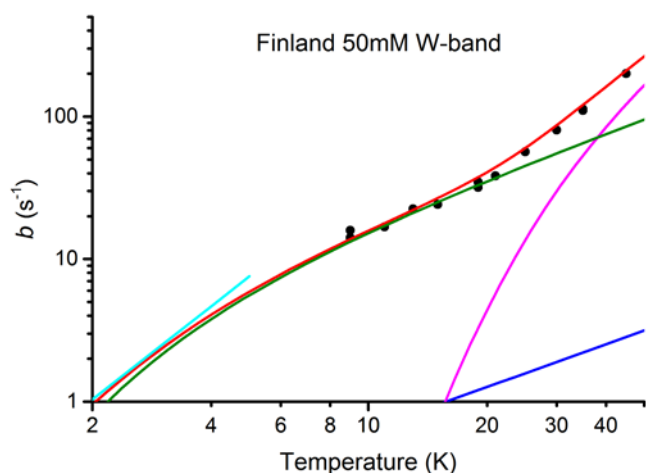

Figure S 2 Plots of the low-temperature spin-lattice relaxation rate *b* for 50 mM Finland trityl at W-band with fits of the direct (blue), Raman (magenta), Orbach-Aminov (green) and total (red) rates from eq. (2). The line in the 2-5 K region is the fit by Filibian et al. (cyan) for 15 mM OX063 in pyruvic acid at W-band between 1.8-4.2 K.

S 3 Temperature and concentration dependence of relaxation

The temperature dependence of OX063 and Finland trityl at each concentration are plotted, Figures S 3-18, along with the best set of fits as described in the paper. All samples used the same stock of solvent and were fit with the same Debye temperature determined from global fits described in the paper and Table 1. The Orbach-Aminov splitting was taken to be a property of the radical being measured. The coefficients of the Raman relaxation term and the direct relaxation term appear to be independent of radical but do depend on the radical and magnetic field used in the measurement. The coefficient of the Orbach-Aminov relaxation term depends on radical concentration, radical and magnetic field. The Finland trityl data were fit well with an Orbach-Aminov coefficient having a quadratic dependence on radical concentration, but the OX063 had to be fit with individual coefficients for the Orbach-Aminov term as described in the paper.
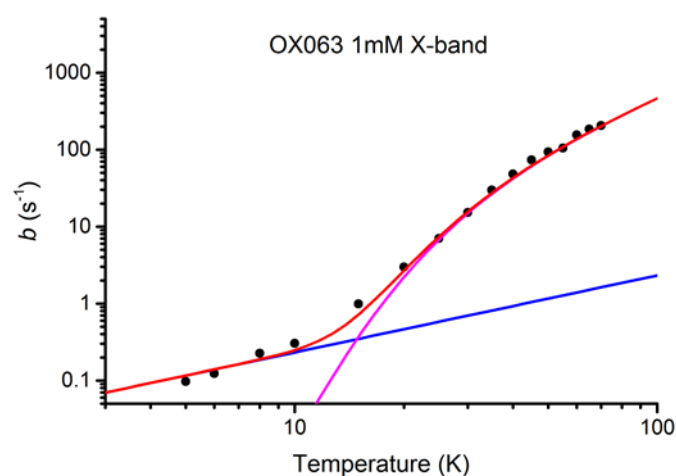

Figure S 3 Temperature dependence of spin-lattice relaxation rate, *b*, of 1 mM OX063 in 60:40 glycerol:H_2O (9.784 GHz, 348.4 mT) showing contributions of the Direct (blue) and Raman (magenta) processes.
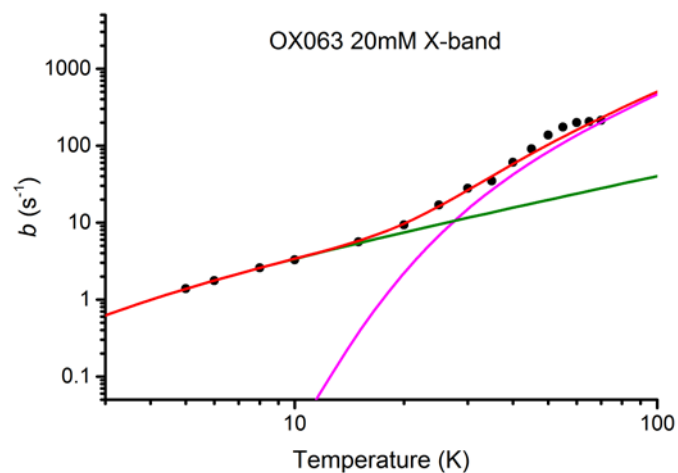
Figure S 4 Temperature dependence of spin-lattice relaxation rate, b, of 20 mM OX063 in 60:40 glycerol:H_2O (9.779 GHz, 348.1 mT) showing contributions of Raman (magenta) and Orbach (green) processes.
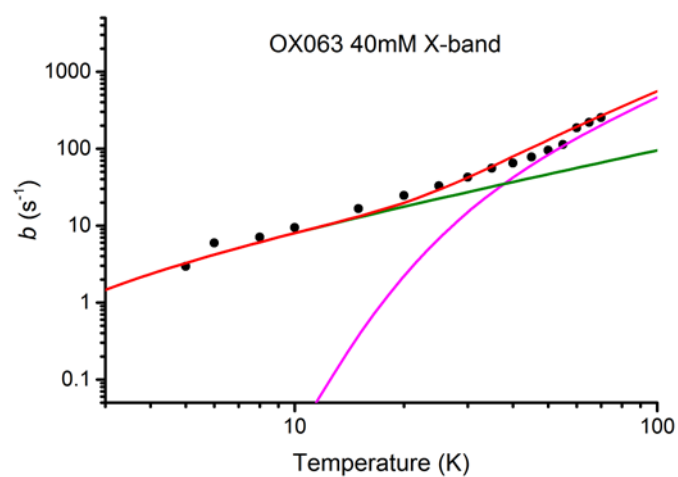

Figure S 5 Temperature dependence of spin-lattice relaxation rate, b, of 40 mM OX063 in 60:40 glycerol:H_2O (9.779 GHz, 348.1 mT) showing contributions of Raman (magenta) and Orbach (green) processes.
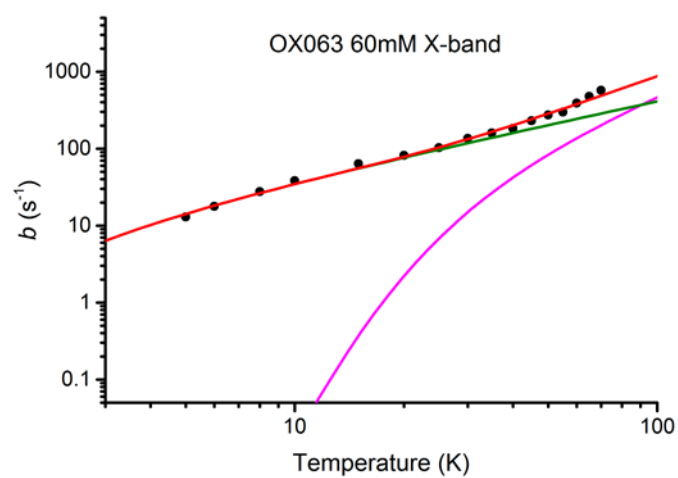

Figure S 6 Temperature dependence of spin-lattice relaxation rate, b, of the freshly frozen sample of 60 mM OX063 in 60:40 glycerol:H_2O (9.786 GHz, 348.4 mT) showing contributions of Raman (magenta) and Orbach (green) processes.
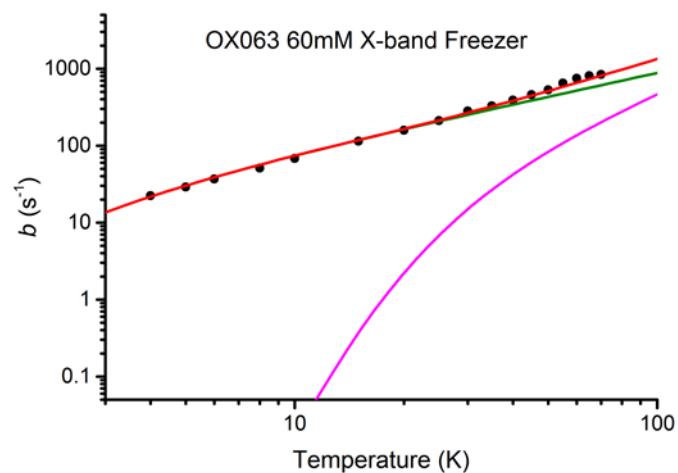
Figure S 7 Temperature dependence of spin-lattice relaxation rate, *b*, of 60 mM OX063 in 60:40 glycerol:H_2O after storage in the freezer (9.785 GHz, 348.4 mT) showing contributions of Raman (magenta) and Orbach (green) processes.
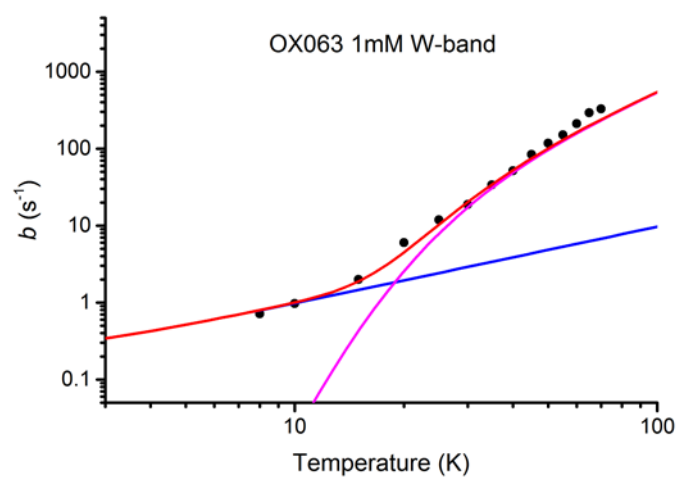

Figure S 8 Temperature dependence of spin-lattice relaxation rate, *b*, of 1 mM OX063 in 60:40 glycerol:H_2O (93.74 GHz, 3362.9 mT) showing contributions of Direct (blue) and Raman (magenta) processes.
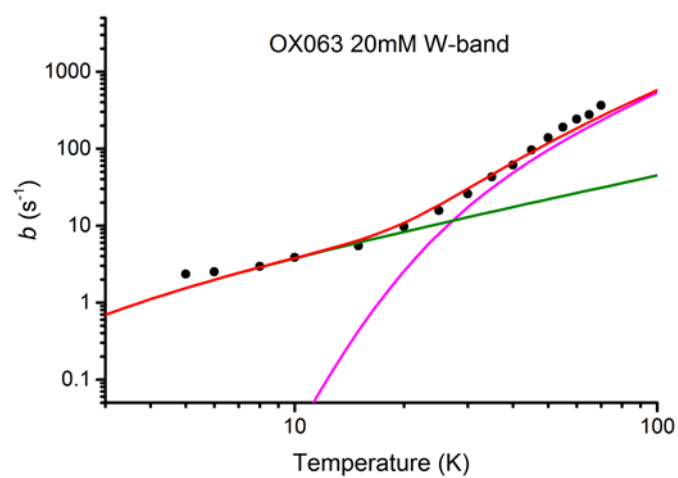

Figure S 9 Temperature dependence of spin-lattice relaxation rate, *b*, of 20 mM OX063 in 60:40 glycerol:H_2O (93.89 GHz, 3365.1 mT) showing contributions of Raman (magenta) and Orbach (green) processes.

Figure S 10 Temperature dependence of spin-lattice relaxation rate, *b*, of 40 mM OX063 in 60:40 glycerol:H_2O (93.93 GHz, 3366.9 mT) showing contributions of Raman (magenta) and Orbach (green) processes.
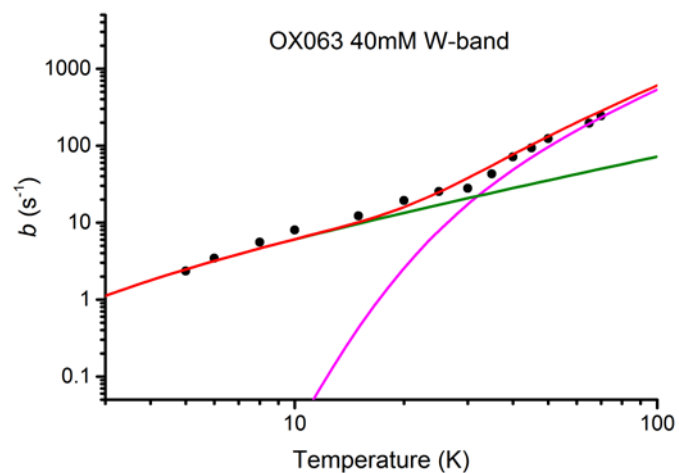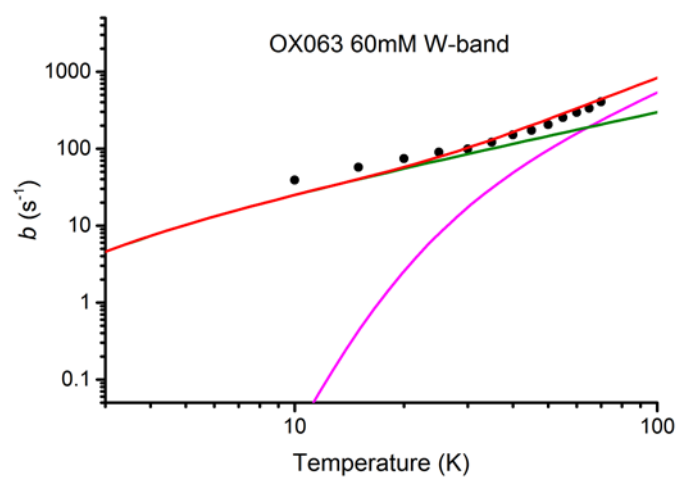

Figure S 11 Temperature dependence of spin-lattice relaxation rate, *b*, of 60 mM OX063 in 60:40 glycerol:H_2O (93.92 GHz, 3366.7 mT) showing contributions of Raman (magenta) and Orbach (green) processes.
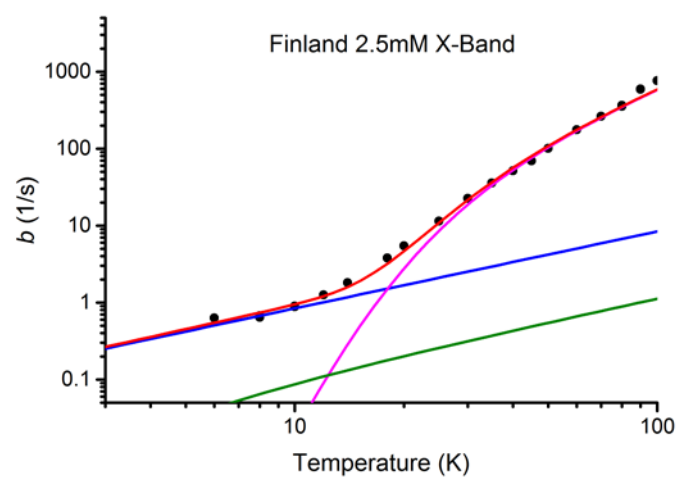

Figure S 12 Temperature dependence of spin-lattice relaxation rate, *b*, of 2.5 mM Finland trityl in 60:40 glycerol:H_2O (9.775 GHz, 348.0 mT) showing contributions of Direct (blue), Raman (magenta) and Orbach (green) processes.

Figure S 13 Temperature dependence of spin-lattice relaxation rate, *b*, of 26 mM Finland trityl in 60:40 glycerol:H_2O (9.781 GHz, 348.1 mT) showing contributions of Direct (blue), Raman (magenta) and Orbach (green) processes.

Figure S 14 Temperature dependence of spin-lattice relaxation rate, *b*, of 50 mM Finland trityl in 60:40 glycerol:H_2O (9.779 GHz, 348.1 mT) showing contributions of Direct (blue), Raman (magenta) and Orbach (green) processes.
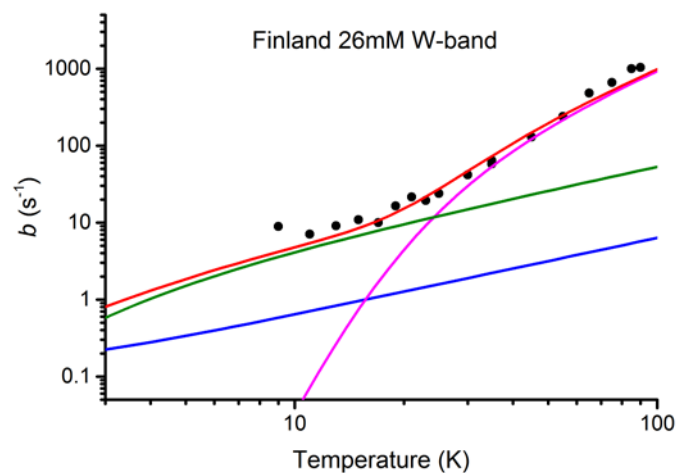

Figure S 15 Temperature dependence of spin-lattice relaxation rate, *b*, of 2.5 mM Finland trityl in 60:40 glycerol:H_2O (94.19 GHz, 3362.0 mT) showing contributions of Direct (blue), Raman (magenta) and Orbach (green) processes.
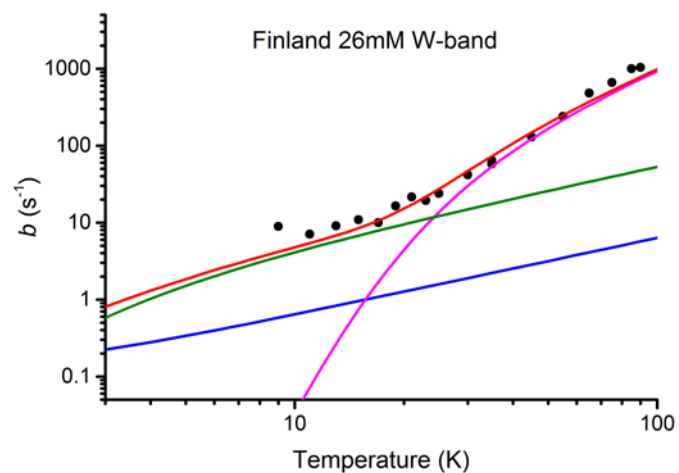
Figure S 16 Temperature dependence of spin-lattice relaxation rate, b, of 26 mM Finland trityl in 60:40 glycerol:H_2O (94.26 GHz, 3363.8 mT) showing contributions of Direct (blue), Raman (magenta) and Orbach (green) processes.

Figure S 17 Temperature dependence of spin-lattice relaxation rate, b, of 39 mM Finland trityl in 60:40 glycerol:H_2O (94.25 GHz, 3363.3 mT) showing contributions of Direct (blue), Raman (magenta) and Orbach (green) processes.
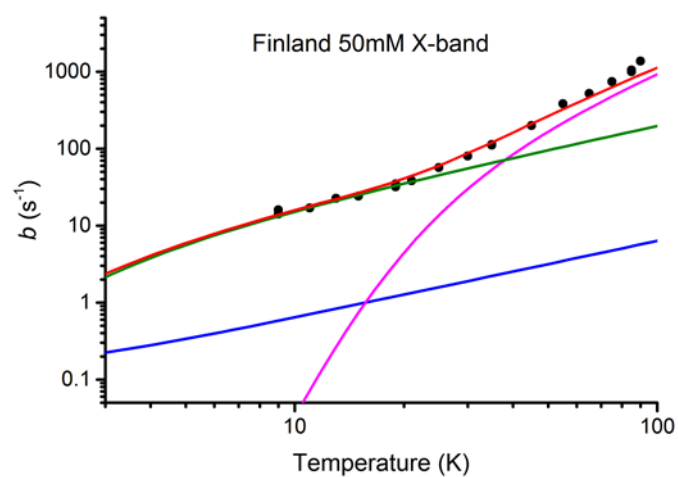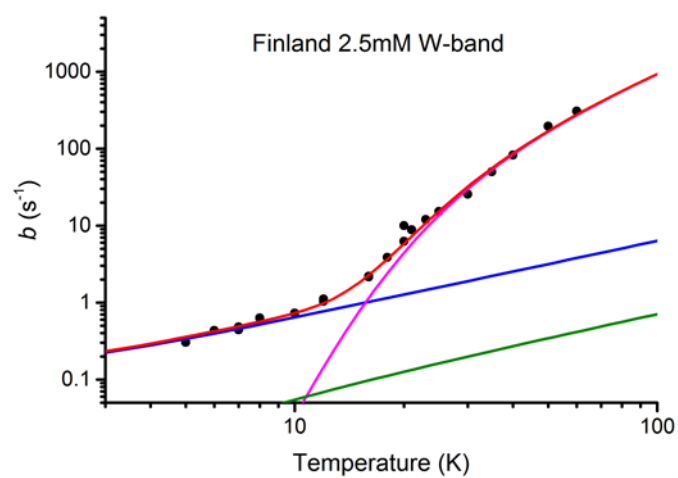

Figure S 18 Temperature dependence of spin-lattice relaxation rate, b, of 50 mM Finland trityl in 60:40 glycerol:H_2O (94.21 GHz, 3362.0 mT) showing contributions of Direct (blue), Raman (magenta) and Orbach (green) processes.
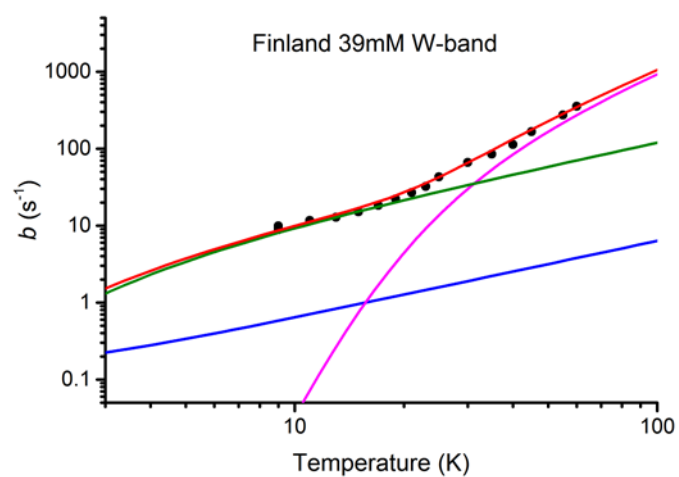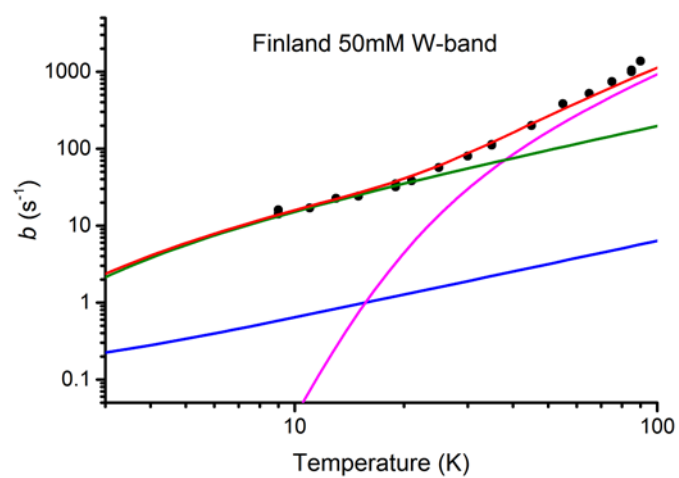
Close examination of the last few high-temperature points in each of the Figures S 3-18 shows some deviation in both directions from the fitted curves. This is an artifact from operation of the sample cryostat with liquid helium when measuring the temperature dependence above 40 K. Efficient use of liquid helium in this regime requires operation with the helium vapor at low density with low heat capacity while the cryostat and resonator have high heat capacities and the temperature is regulated at a location several centimeters from the sample. These conditions are ripe for significant thermal gradients in the cryostat that are sensitive to pressures, flow rates and other operating conditions but tend to be random from one run to another. The temperatures of the last few points at the high end have greater uncertainty than the rest of the points in each figure. Fortunately, this occurs in a region where the relaxation is dominated by the concentration-independent Raman relaxation so that the temperature variations for a sample at one concentration cancel those in a sample at another concentration. The temperature uncertainty at the high temperature region affects the Raman term which is entirely negligible in the range pertinent to dissolution DNP.

S 4 EPR spectral broadening

CW-EPR spectra of the 20-60 mM OX063 samples at 77 K have considerable broadening relative to spectra at low concentration.[3] There is a single sharp line with a pair of weak ^{1}H spin-flip satellite lines approximately the nuclear Zeeman field, 0.5 mT, above and below the main line. The peak-to-peak linewidth of the main line is quite constant in this range of concentrations. But the lineshape shows large changes in the wings as the center line goes from nearly Gaussian in shape at 20 mM to approximately Lorentzian in shape at 60 mM. The ^{1}H spin-flip satellite lines are well resolved from the central line at 20 mM and below, but they are obscured by the wings of the central peak at 40 and 60 mM, Figure S 19.
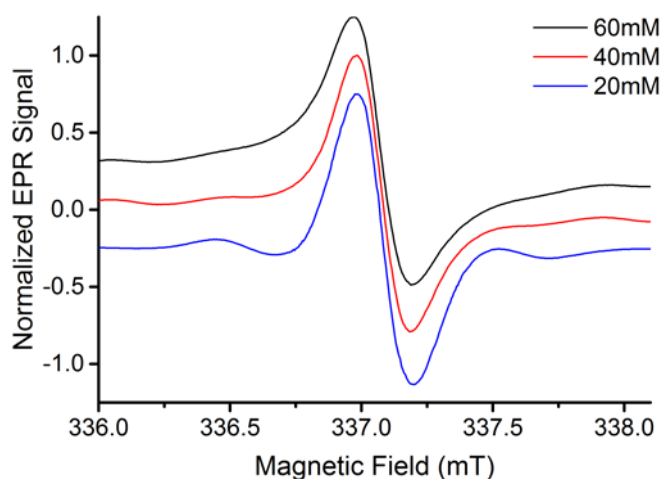

Figure S 19 Concentration dependence of the X-band CW-EPR spectrum of OX063 in 60:40 glycerol:H$_2$O at 77 K. The broadening in the wings of the peak is quite noticeable ~0.3 mT from the center of the spectrum.

S 5 Half-field and third-field EPR transitions

The EPR spectrum of triplets, biradicals and radical pairs often have a relatively narrow line at approximately half of the magnetic field of the center of the 'normal' EPR spectrum. This line is commonly known as the half-field transition and corresponds to the formally forbidden $\Delta m_S = \pm 2$ EPR transition between the pair of $m_S = \pm 1$ levels of a state with S=1, often called a triplet state but it need not be the triplet state of an aromatic, organic molecule. This transition becomes weakly allowed in conventional CW-EPR by the second-order perturbation from S_+^2 and S_-^2 terms in the Zero Field Splitting (ZFS or dipolar) Hamiltonian, even if there is no exchange interaction, J, to produce distinct singlet and triplet states.[5] The total integrated intensity of the half-field transition is much weaker than that of the allowed transitions by a factor proportional to $D^2/(h\nu)^2$.[6] However, the half-field transition is not broadened to first-order by the ZFS interactions while the allowed spectrum is broadened, making the half-field transition detectable in EPR spectra of frozen solutions of many triplet molecules and radical pairs.

Half-field transitions are observed in the CW-EPR spectra of the higher concentration Finland trityl samples, Figure S 20a. The peak to peak linewidth is similar to those of the allowed transitions at g~2, but there is a noticeable growth in the wings of the half-field lines with increasing concentration, as there is for the g~2 lines. Double integration of the half-field transitions is difficult because of their low intensity relative to the noise, but is roughly 10^{-5} times weaker than the g~2 portion of the spectrum, Table S 1. The increasing ratio of double integrals with concentration indicates that states with S>1/2 form by aggregation at higher radical concentrations. The half-field spectra in OX063 samples are similar in shape and intensity to those of Finland trityl samples and are consistent with those reported by Marin-Montesinos, et al.[7, 8] These half-field spectra are

another point of similarity between our samples and those of Marin-Montesinos et al.[7, 8], and indicate significant dipolar interactions among the radicals. But, as shown by Eaton, et al.[5], these half-field spectra provide virtually no information about the clusters formed in the samples; their characterization must come from careful analysis of spin dynamics and spin relaxation.

Table S 1 The ratio of the double integrals of the half-field line to those of the g~2.0 line in samples of OX063 and Finland trityl with concentration. N.D. indicates that a half-field lines was not detected, and an upper limit on the ratio determined by the noise in the spectrum is given in parentheses.

Radical	Concentration	Ratio of Double Integrals
Finland Trityl	1 mM	N.D. ($<1.8*10^{-6}$)
	15 mM	N.D. ($<7.8*10^{-6}$)
	30 mM	$7.5*10^{-6}$
	60 mM	$12.5*10^{-6}$
OX063	20 mM	$3.8*10^{-6}$
	40 mM	$7.1*10^{-6}$
	60 mM	$5.5*10^{-6}$

The half-field transitions of trityl radical aggregates are likely to be exceptions to the general rule that half-field lines are seen only for S=1 states with large D. The half-field line is quite weak because of the factor of $D^2/(h\nu)^2$ but it will be readily detected because of its sharp linewidth. When the ZFS are large, the narrow half-field transition reflects primarily the states with S=1 because half-field transitions other than those between $m_S=\pm1$ levels are broadened by ZFS nearly as much as the allowed transitions. The half-field transitions for S>1 states will not be enormously broadened by ZFS in trityl aggregates so the half-field line can be taken only as an indication of states with S≥1. For trityl radicals, ZFS is comparable to the spectral width of an isolated radical, so the half-field transitions have roughly the same spectral width as the allowed transitions whether from an S=1 state where broadening by ZFS is absent to first order, or from S≥3/2 states where ZFS does broaden half-field lines. The broadening seen in Figure S 20a with increasing concentration has contributions from dipolar broadening from nearby radicals and clusters of radicals and from half-field transitions from clusters larger than pairs with S>1.
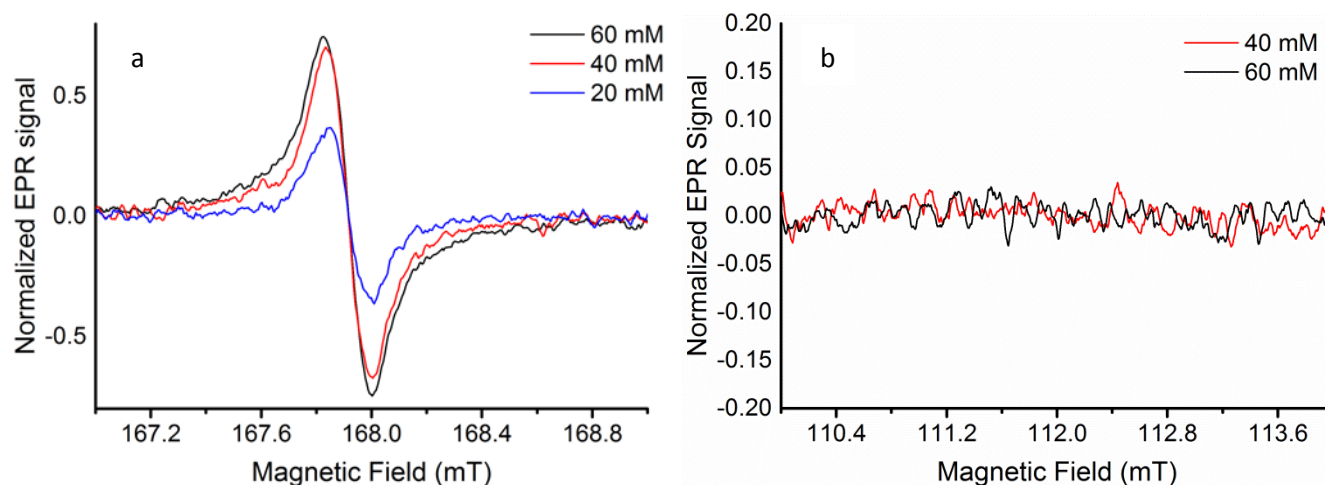

Figure S 20 Half-field and third-field regions of the X-band CW-EPR spectrum of Finland trityl in 60:40 glycerol:H₂O at 77 K. a) Half-field transitions grow and broaden with increasing trityl concentration. b) No signals are detected in the third-field region for 40 or 60 mM radical. Concentrations are indicated by the color of the trace: Blue – 20 mM; Red – 40 mM; Black – 60 mM.

The region for third-field transitions was examined for CW-EPR spectra in the highest concentration Finland trityl samples, Figure S 20b. No indication of any signal is seen at the limit of sensitivity of the spectrometer. This result is expected because the third-field region corresponds to a $\Delta m_S=\pm3$ EPR transition which is forbidden even for second-order perturbation theory by S_+^2 and S_-^2 terms in the Zero Field Splitting (ZFS) Hamiltonian. The third-field transition becomes allowed in conventional CW-EPR only in third-order perturbation theory with a ZFS interaction. Its transition intensity scales as $D^4/(h\nu)^4$, leading us to expect a third-field transition roughly 10^{-10} times weaker than the transition at g~2.0 and well beyond our sensitivity, for instance, in the 60 mM OX063 sample, the third-field transition is much less than $3*10^{-7}$ times the intense than the g~2.0 line.

S 6 Distribution of relaxation rates

The recovery from saturation is non-exponential at all but the lowest radical concentrations. The recovery has the general form $M_z(t) - M_{z,eq} = (M_z(0) - M_{z,eq}) e^{-\sqrt{a*t} - b*t}$ which corresponds to a broad spectrum of relaxation rates given by

$$n(\omega)d\omega = \frac{1}{2}\sqrt{\frac{a}{\pi\,(\omega-b)^3}}\,e^{-\frac{a}{4\,(\omega-b)}}\,d\omega \text{ when } \omega>b \text{ and } 0 \text{ otherwise.}$$

This distribution is plotted, Figure S 21, for different ratios of a/b. The curve for $a/b \sim 0.1$ is representative of the distribution of relaxation rates for OX063 and Finland trityl.
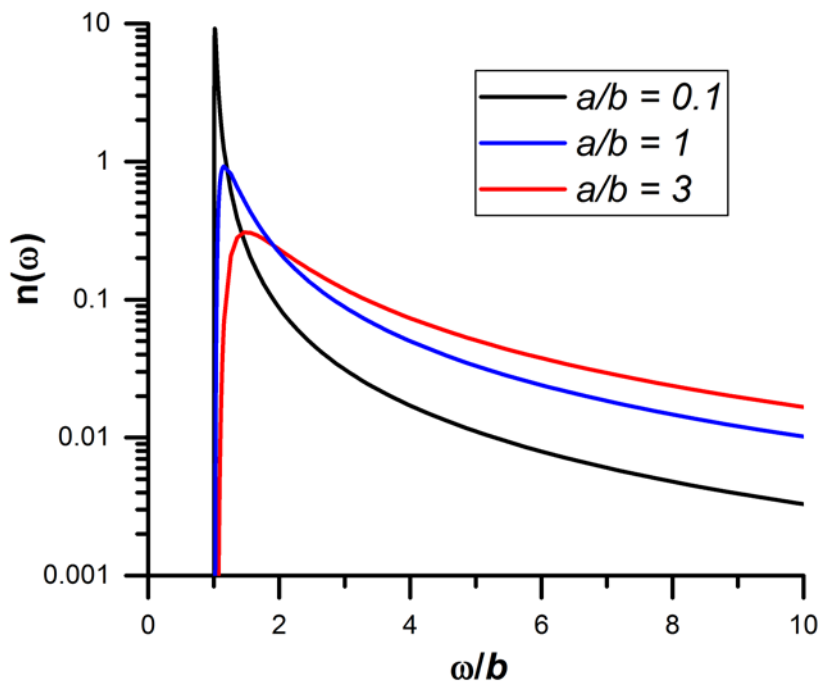

Figure S 21 The distribution of relaxation rates for ratios of a/b of 0.1 (black), 1 (blue) and 3 (red) versus the rate normalized by b.

S 7 Spin Susceptibility

The spin susceptibility, χ, as reported by the double integral of the EPR spectrum is a measure of the number of spins present in a sample. The ZFS of pairs and other aggregates of small free radicals are typically much larger than the linewidth of the individual radicals surrounded by solvent. The centers of the unpaired electron spin distribution are only a few tenths of a nanometer apart so that contact pairs, triads, etc. of such radicals in frozen samples have distinct spectra that are readily separated allowing the χ of the various aggregates to be measured. However, contact pairs of bulky trityl radicals have small ZFS[8] that are similar to ^{1}H spin-flip satellite lines and natural abundance ^{13}C hyperfine splittings[3] or even the dipolar broadening in concentrated samples, Figure S 19.

The χ is unaffected by the exchange interaction, J, between radicals when $|J|<<k_BT$. The total χ of a sample is unaffected by aggregate formation as long as J is small compared to thermal energy. However, as the sample temperature drops so that $|J|\geq k_BT$, the $\chi(T)$ will increase faster than 1/T for aggregates if the exchange is ferromagnetic but $\chi(T)$ will increase more slowly than 1/T, or even decrease, if the exchange is antiferromagnetic. Thus the χ, normalized by sample volume, will be proportional to the total trityl radical concentration if $|J|<<k_BT$. But if aggregates having $|J|\geq k_BT$ form at higher concentrations, χ will not be proportional to total trityl radical concentration.

We examined the χ of Finland trityl and OX063 solutions in 60:40 glycerol:water over a concentration range of 1-60 mM which includes a concentration range where optical measurements showed changes in aggregation at room temperature.[7, 8] Different concentrations were produced by serial dilution and loaded into capillaries. Relative sample volumes were estimated from the sample lengths, but the meniscus causes some uncertainty in volumes. CW EPR spectra of the samples were measured at room temperature (RT) and at 77 K in liquid nitrogen and the χ, normalized by volume were determined from double integration of the g~2.0 spectrum. The χ(RT) is proportional to the concentration from 0-60 mM for both Finland trityl and OX063, Figure S 22.
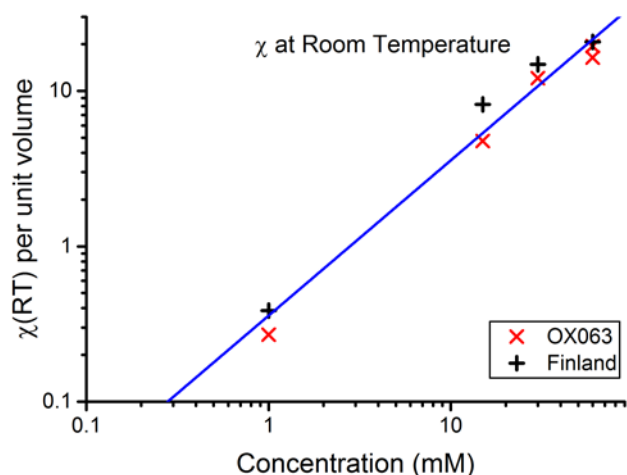
Figure S 22 The χ(RT) versus radical concentration for **+**: Finalnd trityl and **X**: OX063 in 60:40 glycerol:water at X-band where consistent tuning of the cavity could be maintained. The blue line is a least-squares fit (R^2>0.94) of a straight line passing through the origin to data of both radicals.

The linear relationship between χ(RT) and total trityl concentration indicates no aggregates with $|J| \geq k_B T$ form. A plot of χ(77 K) versus χ(RT), Figure C 23, also shows a good linear relation passing through the origin. These χs were not normalized by sample volume, so that no errors are introduced by sample volume uncertainty. The numerical scale is not corrected for differences in measurement conditions, such as microwave power and modulation amplitude. The linear relationship between χ(77 K) and χ(RT), extending through the origin, indicates that aggregates formed in any significant amount at radical concentrations below 60 mM have $|J| \ll k_B$(77 K). This is in complete agreement with the indication from the Orbach-Aminov relaxation term that Θ_{Orb}~3.5-5.5 K for triads of both radicals.

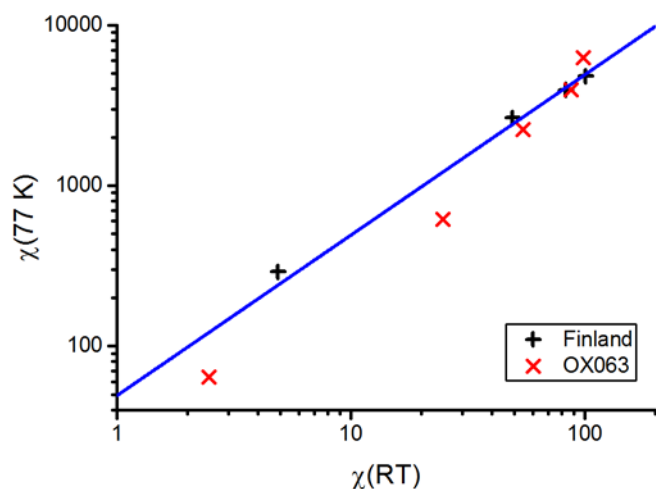Figure S 23 The χ(77 K) versus χ(RT) for **+**: Finalnd trityl and **X**: OX063 in 60:40 glycerol:water at X-band where consistent tuning of the cavity could be maintained. The blue line is a least-squares fit (R^2>0.95) of a straight line passing through the origin to data of both radicals.

References

1.   M. K. Bowman, C. Mailer and H. J. Halpern, *J. Magn. Reson.*, 2005, **172**, 254-267.

2.   A. J. Fielding, P. J. Carl, G. R. Eaton and S. S. Eaton, *Appl. Magn. Reson.*, 2005, **28**, 231-238.

3.   S. N. Trukhan, V. F. Yudanov, V. M. Tormyshev, O. Y. Rogozhnikova, D. V. Trukhin, M. K. Bowman, M. D. Krzyaniak, H. Chen and O. N. Martyanov, *J. Magn. Reson.*, 2013, **233**, 29-36.

4.   M. Filibian, S. C. Serra, M. Moscardini, A. Rosso, F. Tedoldi and P. Carretta, *Phys. Chem. Chem. Phys.*, 2014, **16**, 27025-27036.

5.   S. S. Eaton, K. M. More, B. M. Sawant and G. R. Eaton, *J. Am. Chem. Soc.*, 1983, **105**, 6560-6567.

6.   M. S. de Groot and J. H. van der Waals, *Mol. Phys.*, 1960, **3**, 190-200.

7.   I. Marin-Montesinos, J. C. Paniagua, A. Peman, M. Vilaseca, F. Luis, S. Van Doorslaer and M. Pons, *Phys. Chem. Chem. Phys.*, 2016, **18**, 3151-3158.

8.   I. Marin-Montesinos, J. C. Paniagua, M. Vilaseca, A. Urtizberea, F. Luis, M. Feliz, F. Lin, S. Van Doorslaer and M. Pons, *Phys. Chem. Chem. Phys.*, 2015, **17**, 5785-5794.